Hindawi Publishing Corporation
International Journal of Photoenergy
Volume 2012, Article ID 398508, 8 pages
doi:10.1155/2012/398508

Research Article

Enhanced Photoactivity of Fe + N Codoped Anatase-Rutile TiO_2 Nanowire Film under Visible Light Irradiation

Kewei Li,[1,2] Haiying Wang,[1,2,3] Chunxu Pan,[3] Jianhong Wei,[3] Rui Xiong,[3,4] and Jing Shi[3]

[1] *Department of Communication Engineering, Chengdu Institute of Technology, Chengdu 611730, China*
[2] *Intel-cec joint Lab, Institute of IC Mannufacturing Engineering, Chengdu 611730, China*
[3] *Key Laboratory of Artificial Micro- and Nanostructures of Ministry of Education and School of Physics and Technology, Wuhan University, Wuhan 430072, China*
[4] *Ministry of Education Key Laboratory for the Green Preparation and Application of Functional Materials, Hubei University, Wuhan 430072, China*

Correspondence should be addressed to Haiying Wang, wanghaiy@whu.edu.cn and Rui Xiong, xiongrui@whu.edu.cn

Received 9 January 2012; Revised 22 February 2012; Accepted 22 February 2012

Academic Editor: Baibiao Huang

Rutile-anatase phase mixed Fe + N codoped TiO_2 nanowires were designed and prepared by a two-step anodic oxidation method. The results of X-ray diffraction, scanning electron microscopy, and high-resolution transmission electron microscopy confirm that the prepared Fe + N codoped TiO_2 nanowires exhibit intimately contacted anatase-rutile heterostructure with the rutile content of 21.89%. The X-ray photoelectron spectroscopy measurements show that nitrogen and iron atoms are incorporated into the titania oxide lattice, and the UV-visible absorption spectra show that the codoping of iron and nitrogen atoms could extend the absorption to visible light region. The photocatalytic activities of all the samples were evaluated by photocatalytic degradation of methylene blue under visible light irradiation. The Fe + N codoped sample achieves the best response to visible light and the highest photocatalytic activities. The enhancement of photocatalytic activity for Fe + N codoped sample should be ascribed to the synergistic effects of codoped nitrogen and iron ions and the anatase-rutile heterostructure.

1. Introduction

Titanium oxide is a multifunctional material with a wide variety of potential applications including solar cell [1], photocatalyst [2], water splitting [3], and gas sensors [4]. However, the wide band gap of TiO_2 (3.2 eV for the anatase phase and 3.0 eV for the rutile phase) requires ultraviolet (UV) light for electron-hole separation, which is only 5% of the natural solar light [5]. It is of great significance to develop photocatalysts that can be used in visible light region to improve the photocatalytic efficiency. Numerous attempts have been made to optimize the band gap of TiO_2 by different doping schemes, for example, nonmetal doping (such as C, S, N, I [6–11]), metal doping (such as Fe, V, Cr, Nb [12–15]), and nonmetal-metal codoping (such as Mo + C codoping [16], Mo + N codoping [17], Pr + N codoping [18], and Cd + N codoping [19]), to improve the photocatalytic activity. As a result, it was found that the monodoping can generate the recombination center inside the TiO_2, which goes against the light-induced charge carriers' migration to the surface [16, 20]. In compensated n-p codoping systems, the defect bands can be passivated and will not be effective as carrier recombination centers [16, 21] and the Columbic attraction between the n- and p-type dopants with opposite charge substantially enhances doping concentration [22]. Recently, noncompensated codoping was proposed by Zhu et al., for its distinctive merit of ensuring the creation of intermediate electronic bands in the gap region and enhancing photoactivity manifested by efficient electron-hole separation in the visible-light region [23].

It is well-known that powders consisting of anatase and rutile (a classical reference materials is Degussa P25, a mixture of 20% rutile, and 80% anatase) possess higher photoactivity than those of pure anatase. It was thought that the anatase-rutile heterojunction inside the TiO_2 was the main reason for enhanced photoactivity [24]. Deák et

al. calculated the band structure of rutile and anatase and validated that both bands of rutile lie higher than those of anatase, so in mixed systems, the holes are accumulated in the former while the electrons in the latter [25]. As pointed out earlier, the charge separation will enhance the photochemical activity of mixed phase TiO_2 powders.

New interesting issue: does the noncompensated codoping with rutile-anatase mixing phase improve the visible light photocatalytic activity? It was reported that Fe-doped TiO_2 and N-doped TiO_2 exhibit enhanced visible light photocatalytic activity as compared to undoped TiO_2, while Fe + N codoping is the noncompensated codoping, but the light photocatalytic activity is seldom reported. Thus, in this study, Fe + N codoped TiO_2 nanowires with rutile-anatase mixed phase were designed and prepared. Compared with the undoped, Fe-doped and N-doped TiO_2, Fe + N codoped TiO_2 gains the best photocatalytic activity under visible light irradiation and the mechanism of enhanced visible-light photocatalytic activity is discussed in detail.

2. Experimental Section

Titanium foils (0.6 mm thick, 99.5% purity, and cut in 1 cm × 2 cm) were used as the substrates for the growth of the TiO_2 nanowire arrays. The titanium sheets were cleaned by sonicating in 1 : 1 acetone and ethanol solution, followed by being rinsed with deionized water and dried in airstream. The anodization was carried out in a two-electrode electrochemical cell with a graphite sheet as the cathode at a constant potential 60 V. A DC power supply (WYK-6010, 0–60 V, and 0–10 A) was used to control the experimental current and voltage for 1 h. The electrolyte contained 0.5 wt% NH_4F, 5 mL H_2O, and 195 mL ethylene glycol. After anodization, the specimens were cleaned in 10% HCl by ultrasonic immediately for 10 minutes and dried in airstream. The anodization process was repeated for several times.

The samples were then rinsed by ethanol for 5 minutes, after which some of them were submerged in 1.5×10^{-3} mol/L $Fe(NO_3)_3$ solutions for 40 minutes for Fe doping. Postannealing in air at 700°C was employed to remove most of the organic and inorganic species encapsulated in the arrays and transform the amorphous titania to nanocrystalline TiO_2. Nitrogen doping was carried out by annealing the samples in ammonia atmosphere at 500°C. The reagents—acetone (CH_3COCH_3), ethanol (C_2H_5OH), ammonium fluoride (NH_4F), $Fe(NO_3)_3$, and ethylene glycol ($C_2H_6O_2$) were of analytical-grade without further purification.

The crystal structures of samples were characterized by X-ray diffraction (XRD, Bruker AXS D8 Advance diffractions) using Cu K_α radiation. The surface morphologies of the nanowire arrays were observed by scanning electron microscopy (SEM, S-4800) and high-resolution transmission electron microscopy (TEM 2010FEF HRTEM, JEOL, Japan). The X-ray photoelectron spectroscopy (XPS) experiments were performed on a VG Multilab2000 spectrometer to obtain the information on chemical binding energy of the TiO_2 nanowires which was calibrated with the reference to the C 1s peak at 284.6 eV. The UV-visible absorption spectra were measured using a Cary 5000 UV-Vis-NIR spectrophotometer; $BaSO_4$ was used as a reectance standard in a UV-visible diffuse reectance experiment. The photocatalytic activities under visible light irradiation were evaluated by the degradation of methyl blue irradiated by a 450 W xenon lamp. In the process, a TiO_2 nanowire array with dimensions of 0.5 cm × 0.5 cm was immersed into 3 mL 10 mg/L methyl blue (MB) solution and placed below xenon lamp with 10 cm distance. The solution in the photoreactor was placed in dark for 30 minutes to reach the absorption-desorption equilibrium of the dye molecules on the sample surface.

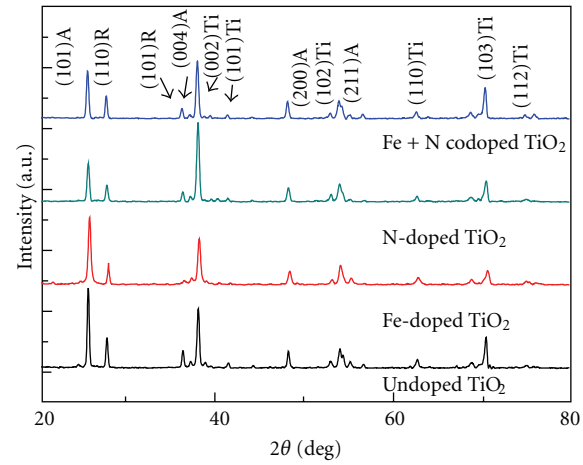

Figure 1: X-ray diffraction patterns of undoped, Fe-doped, N-doped, and Fe + N codoped TiO_2 nanowires.

3. Results and Discussions

Figure 1 shows the XRD patterns of the undoped, Fe-doped, N-doped, and Fe + N codoped polycrystalline TiO_2 samples. Compared with the standard patterns of the anatase phase TiO_2 (JCPDS 21-1272) and the rutile phase (JCPDS 21-1276), no peaks of impurities are detected except the peaks of metal titanium coming from the substrates. The contents of rutile phase and anatase phase are calculated by the XRD results, using the method described by Zhu et al. [26] and listed in Table 1. The results show that the content of rutile phase in Fe-doped TiO_2 (19.66 wt%) is lower than that of the undoped TiO_2 (21.88 wt%), that is to say, the content of rutile decreases for the iron doping after the heating treatment, which indicates that the doping of iron may retard the transition from anatase to rutile. The content of rutile in the N-doped and Fe + N codoped TiO_2 are 22.48 wt% and 21.89 wt%. The average crystallite sizes were calculated by Scherrer's formula ($D = k\lambda/\beta\cos\theta$, $k = 0.89$, $\lambda = 0.15418$ nm) and listed in Table 1, choosing the peaks at scattering angles of 25° and 27.5° for anatase and rutile, respectively. The average crystallite sizes for anatase phase in the undoped TiO_2 and samples doped with Fe, N, Fe + N are 32.92 nm, 25.27 nm, 27.60 nm, and 27.78 nm, while the average crystallite sizes for rutile phase are 30.57 nm, 25.30 nm, 26.93 nm, and 28.78 nm, respectively. These results

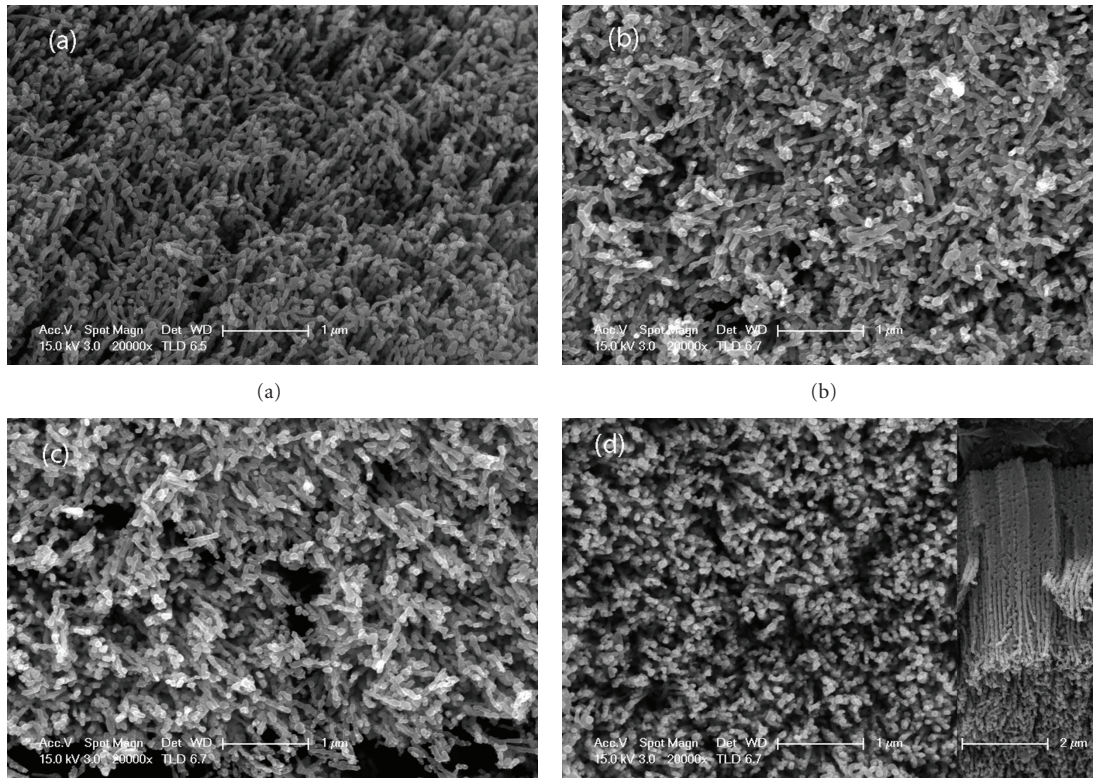

Figure 2: SEM images of (a) the undoped, (b) Fe-doped, (c) N-doped, and (d) Fe + N codoped TiO_2 nanowires.

Table 1: The average crystallite size of anatase TiO_2 and the content of rutile, anatase for undoped, Fe-doped, nitrogen-doped, and Fe + N codoped TiO_2 nanowires.

	Undoped TiO_2	Fe-doped TiO_2	N-doped TiO_2	Fe + N codoped TiO_2
Content of rutile (wt%)	21.88	19.66	22.48	21.89
Content of anatase (wt%)	78.12	80.34	77.52	78.11
Average crystallite size of anatase (nm)	32.92	25.27	27.60	27.78
Average crystallite size of rutile (nm)	30.57	25.30	26.93	28.78

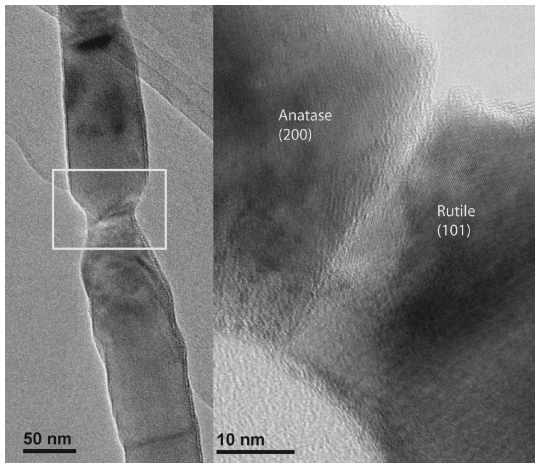

Figure 3: The HRTEM images of Fe + N codoped TiO_2 with magnified local image in the right.

reveal that doping with Fe and N element will retard the growth of the crystallite sizes, which is similar to those described in [27, 28].

Figures 2(a), 2(b), 2(c), and 2(d) present the illustrative top SEM images of typical undoped, Fe-doped, N-doped, and Fe + N codoped TiO_2 samples. The right part of Figure 2(d) is the SEM image of cross section of the Fe + N codoped sample. As it can be seen, the length and the diameter of all the samples are about 5 μm and 90 nm. The nanowires are arranged one by one closely, ensuring that light can be effectively scattered by the rutile phase in the mixing-phase films [29].

The crystalline structure of TiO_2 is further examined by HRTEM. The HRTEM images of a single Fe + N codoped TiO_2 nanowire and the magnied local image in the white rectangle zone is shown in Figure 3. HRTEM observations reveal that the diameter of the nanoparticles is in a size range of 70–100 nm and TiO_2 nanoparticles can be discriminated

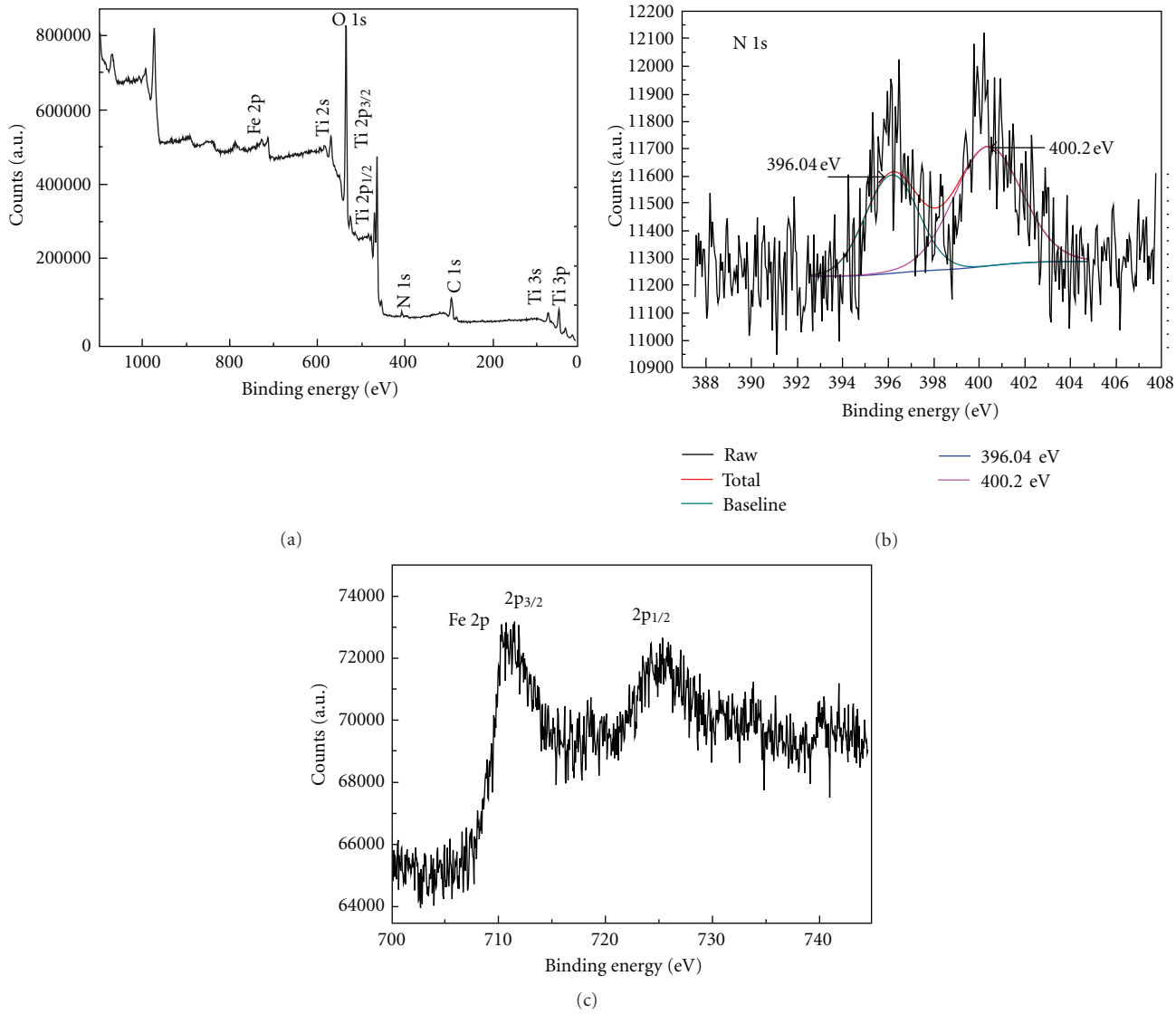

Figure 4: XPS spectra of (a) survey spectrum, (b) N 1s, and (c) Fe 2p for Fe + N codoped TiO_2.

and exhibit a perfect lattice. As shown in Figure 3, the clear anatase-rutile interface is conrmed by HRTEM, where the lattice spaces are measured to be 0.189 nm along the (200) plane of anatase phase and 0.248 nm along the (101) plane of rutile phase, respectively. The formation of intimate contact between anatase and rutile phases is realized so that the charge transfer between the two phases can occur smoothly [30]. The anatase-rutile interface is the active site for photocatalysis and is one of the dominate factors for the enhancement of the photocatalytic activity reported elsewhere [31].

To investigate the composition and the chemical state of ions, XPS measurements were performed. Figure 4(a) is the XPS survey spectrum of the Fe + N sample. The sharp peaks at 284.7 eV, 458.60 eV, 530.15 eV are corresponding to the binding energy of C 1s, Ti $2p_{3/2}$, O1s, and the two weak photoelectron peaks at 710.41 eV and 396.00 eV correspond to Fe $2p_{3/2}$, and N 1s, respectively. The peak at 284.7 eV, in general, is a signal of adventitious elemental carbon as reported in other works [32, 33]. No other impurity peaks were observed, which reveals that the sample contains Ti, O, Fe, and N four elements.

Figure 4(b) is the N 1s core level spectra of Fe + N codoped TiO_2. It is found that there are two peaks with similar intensity at the bonding energies of 396.04 eV and 400.20 eV, respectively. Generally, the peak at 396 eV reflects the formation of N–Ti–O bonds, indicating the substitution of N ion for O ion [34–36]. The peak at 400 eV can be assigned to molecular nitrogen bonded to the surface defects or the N atoms bonding to O sites in TiO_2, forming Ti–O–N bonds [37]. Figure 4(c) shows the high-resolution Fe 2p core level spectrum. As it can be seen, the binding energies of the Fe 2p XPS peaks are at 710.41 eV, indicating that the Fe element in the sample exists mainly in the +3 oxidation state [38]. The peak position of Fe + N codoped TiO_2 exhibits a shift about 0.3 eV to lower energy compared

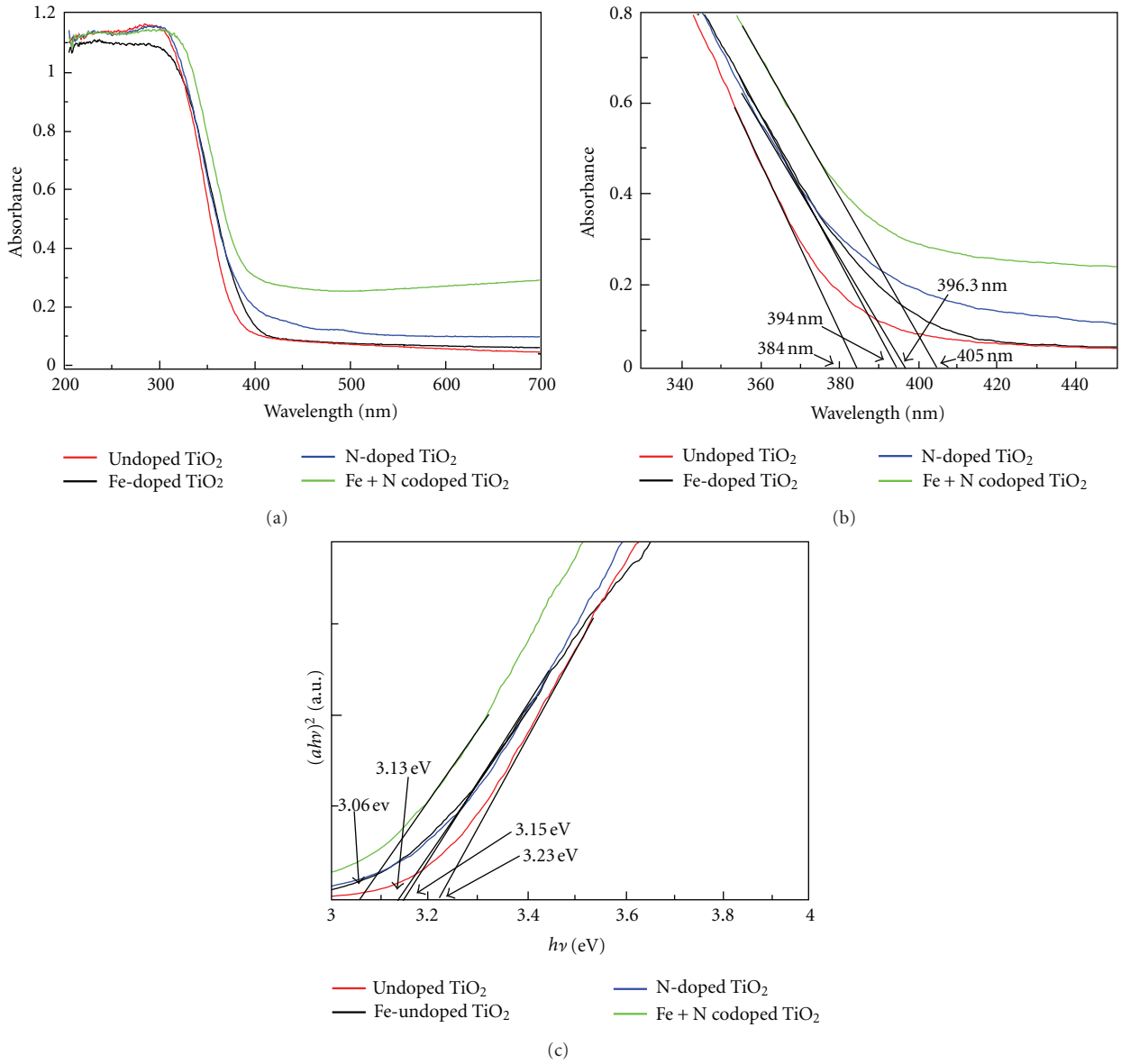

FIGURE 5: UV-vis absorption spectroscopy of undoped, Fe-doped, N-doped, and Fe + N codoped TiO_2 with the wavelength in the range of (a) 200–700 nm, (b) 330–450 nm, and (c) $(\alpha h\nu)^2$ versus $h\nu$ curves.

with that in Fe_2O_3 (710.7 eV for Fe $2p_{3/2}$) [38]. The variation in the elemental binding energy due to the difference in the chemical potential and polarizability of Fe ions in Fe + N codoped TiO_2 and Fe_2O_3 indicates that Fe^{3+} ion has incorporated into the TiO_2 lattice and Fe–O–Ti bonds form in the Fe + N codoped sample [39]. The calculations of the N 1s core level spectrum and Fe 2p core level spectrum show that the N and Fe content is 3.15% and 1.09%, respectively.

Figure 5(a) illustrates the UV-vis absorption spectroscopy of the undoped, Fe-doped, N-doped, and Fe + N codoped TiO_2. The undoped TiO_2 exhibits the characteristic spectrum of TiO_2 with its fundamental absorption sharp edge around 380 nm. Compared with the undoped TiO_2, the absorption edge is shifted toward visible light range for Fe-doped, N-doped, and Fe + N codoped samples and a significant enhancement of absorption visible light range is observed in N-doped and Fe + N codoped samples. As it can be seen from Figure 5(a), the spectrum of Fe + N codoped sample has the largest red-shift. The local spectra (Figure 5(b)) indicate that the onset of the absorption spectrum appears at 384 nm, 394 nm, 396.3 nm, and 405 nm, for undoped, Fe-doped, N-doped, and Fe + N codoped TiO_2, respectively. According to the equation $\lambda = 1240/E_g$, the band gaps of the undoped, Fe-doped, N-doped, and Fe + N codoped TiO_2 are 3.23 eV, 3.15 eV, 3.13 eV, and 3.06 eV. Figure 5(c) shows the plots of $(\alpha h\nu)^2$ versus $h\nu$ deduced from Figure 5(a). The band gap of each samples is determined by fitting the absorption spectra data according to the equation $(\alpha h\nu)^2 = B(h\nu - E_g)$ (α is the absorption coefficient; $h\nu$ is the photo energy; B is a constant number; and E_g is

the absorption band gap energy). As it can be seen that the band gaps of the undoped, Fe-doped, N-doped, and Fe + N codoped TiO_2 are 3.23 eV, 3.15 eV, 3.13 eV, and 3.06 eV, which are consistent with the results of Figure 5(b) and similar to those reported in [40, 41], but much higher than the values calculated by Romero-Gomez et al. [23]. The reason for this deviation may be that the doping content in experiments is much lower than that in the theoretical model.

As to the origin of visible-light sensitivity in Fe, N and Fe + N codoped TiO_2, the possible mechanism can be proposed. It is known that the band gap of TiO_2 can be tailored by doping with some nonmetal or metal elements. Herein, for the Fe-doped sample, the absorption edge red-shift could be understood by the band gap narrowing, which is the result of the induced sub-band-gap transition corresponding to the excitation of 3d electrons of Fe^{3+} to TiO_2 conduction band [41, 42]. In nitrogen doped sample, the doped N ions could induce an add-on shoulder on the edge of the valence band maximum and the localized N 2p states above the valence band [40]. On the other hand, it is known that N has a lower valence state than O so that the incorporation of N must promote the synchronous formation of oxygen vacancies for the charge equilibrium in TiO_2 [43]. Therefore, the band narrowing due to newly formed oxygen vacancies by N-doping in TiO_2 cannot be neglected. As a result, the visible light response for N-doped TiO_2 is attributed to both oxygen vacancies and the N 2p states. For Fe + N codoped sample, compared with the N-doped TiO_2, the Fe element is introduced into the lattice of TiO_2 as the oxide state of Fe^{3+} by above discussion, so that Fe-doping is a p-type doping and can increase the oxygen vacancies induced by the hole doping of N, similar as [43]. Consequently, the codoped TiO_2 results in the best response to visible-light and the largest red-shift because of the synergistic effect of Fe and N codopant.

To evaluate the photocatalytic activities of the undoped, Fe-doped, N-doped, and Fe + N codoped samples, experiments were carried out for MB degradation in an aqueous solution under visible light irradiation by insert a filter ($\lambda \geqq 400$ nm) between the Xe-lamp and the samples. Figure 6 shows the photocatalytic degradation curves of MB catalyzed by the samples. The photocatalytic activity is in the order of the Fe + N codoped TiO_2 > N-doped TiO_2 > Fe-doped TiO_2 > undoped TiO_2. The Fe + N codoped TiO_2 shows the best photocatalytic activity and leads to a removal of MB up to 57.42% in 4 hours.

It has been reported that oxygen vacancy induced by N doping or self-doping plays an important role in the photocatalytic activity of TiO_2 catalyst by trapping the photoinduced electron and acting as a reactive center for the photocatalytic process [44, 45]. Fe + N codoping on the photocatalytic activity in anatase-rutile mixed TiO_2 nanowires, p-type Fe doping can increase the oxygen vacancies in N-doped TiO_2 so that the photocatalytic activity of the sample is enhanced after introducing Fe^{3+} to form the Fe + N codoped sample. It is known that the minimum of the conduction band of the rutile phase lies at higher in energy than that of the anatase phase by about 0.3-0.4 eV [25].

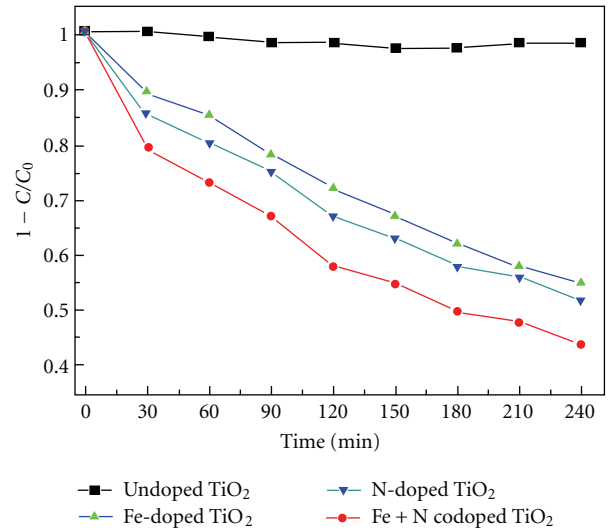

Figure 6: Degradation curves of MB for the undoped, Fe-doped, N-doped, and Fe + N codoped samples.

The Fe^{3+} energy level is just below the conduction band of anatase [41, 42]. The nitrogen doping could induce an add-on shoulder on the edge of the valence band maximum and the localized N 2p states above the valence band [40]. Therefore, after Fe + N codoping, the anatase-rutile mixed TiO_2 nanowires have complex band lineup, similar with the band lineup of rutile and anatase [25]. This complex staggered alignment of the bands effectively enhances the charge separation with migrating holes accumulating in rutile while electrons in anatase, thus enhancing photocatalytic activity, accordingly.

4. Conclusions

In conclusion, TiO_2 nanowires with mixed rutile-anatase phase were synthesized by a two-step anodic oxidation method. Doping with nitrogen or iron could enhance the visible light absorption and the photocatalytic activity of TiO_2 nanowires. The Fe + N codoped TiO_2 nanowire possesses the highest visible light absorption and the best photocatalytic activity for catalyzing the degradation of methylene blue. The increase of the quantity of O vacancy and the enhancement of the charge separation in the nanowires due to the complex staggered alignment of the bands leading by Fe and N codoping may be two of the reasons for the increase of photocatalytic activity in the Fe + N codoped sample.

Acknowledgments

The authors would like to acknowledge the financial support from the National Basic Research Program (973 Program) (no. 2009CB939704 and no. 2009CB939705), the National Natural Science Funds (no. 51172166, 10974148, 61106005), National Science Fund for Talent Training in Basic Science (no. J0830310), and Ministry of Education Key Laboratory for the Green Preparation and Application of Functional Materials (Hubei University).

References

[1] C.-C. Wu, Y.-J. Zhuo, P.-N. Zhu, B. Chi, J. Pu, and J. Li, "Tunable fabrication of TiO_2 nanotube arrays with high aspect ratio and its application in dye sensitized solar cell," *Journal of Inorganic Materials*, vol. 24, no. 5, pp. 897–901, 2009.

[2] S. Sreekantan, R. Hazan, and Z. Lockman, "Photoactivity of anatase-rutile TiO_2 nanotubes formed by anodization method," *Thin Solid Films*, vol. 518, no. 1, pp. 16–21, 2009.

[3] Y. Liu, B. Zhou, J. Bai et al., "Efficient photochemical water splitting and organic pollutant degradation by highly ordered TiO_2 nanopore arrays," *Applied Catalysis B*, vol. 89, no. 1-2, pp. 142–148, 2009.

[4] M. H. Seo, M. Yuasa, T. Kida, J. S. Huh, K. Shimanoe, and N. Yamazoe, "Gas sensing characteristics and porosity control of nanostructured films composed of TiO_2 nanotubes," *Sensors and Actuators B*, vol. 137, no. 2, pp. 513–520, 2009.

[5] X. Chen and S. S. Mao, "Titanium dioxide nanomaterials: synthesis, properties, modifications and applications," *Chemical Reviews*, vol. 107, no. 7, pp. 2891–2959, 2007.

[6] X. Yang, C. Cao, K. Hohn et al., "Highly visible-light active C- and V-doped TiO_2 for degradation of acetaldehyde," *Journal of Catalysis*, vol. 252, no. 2, pp. 296–302, 2007.

[7] T. Ohno, M. Akiyoshi, T. Umebayashi, K. Asai, T. Mitsui, and M. Matsumura, "Preparation of S-doped TiO_2 photocatalysts and their photocatalytic activities under visible light," *Applied Catalysis A*, vol. 265, no. 1, pp. 115–121, 2004.

[8] R. Asahi, T. Morikawa, T. Ohwaki, K. Aoki, and Y. Taga, "Visible-light photocatalysis in nitrogen-doped titanium oxides," *Science*, vol. 293, no. 5528, pp. 269–271, 2001.

[9] C.-C. Hu, T.-C. Hsu, and L.-H. Kao, "One-step cohydrothermal synthesis of nitrogen-doped titanium oxide nanotubes with enhanced visible light photocatalytic activity," *International Journal of Photoenergy*, vol. 2012, Article ID 391958, 9 pages, 2012.

[10] Y.-C. Tang, X.-H. Huang, H.-Q. Yu, and L.-H. Tang, "Nitrogen-doped TiO_2 photocatalyst prepared by mechanochemical method: doping mechanisms and visible photoactivity of pollutant degradation," *International Journal of Photoenergy*, vol. 2012, Article ID 960726, 10 pages, 2012.

[11] V. Štengl and T. M. Grygar, "The simplest way to iodine-doped anatase for photocatalysts activated by visible light," *International Journal of Photoenergy*, vol. 2011, Article ID 685935, 13 pages, 2011.

[12] S. Klosek and D. Raftery, "Visible light driven V-doped TiO_2 photocatalyst and its photooxidation of ethanol," *Journal of Physical Chemistry B*, vol. 105, no. 14, pp. 2815–2819, 2002.

[13] H. Kato and A. Kudo, "Visible-light-response and photocatalytic activities of TiO_2 and SrTiO3 photocatalysts codoped with antimony and chromium," *Journal of Physical Chemistry B*, vol. 106, no. 19, pp. 5029–5034, 2002.

[14] K. T. Ranjit and B. Viswanathan, "Synthesis, characterization and photocatalytic properties of iron-doped TiO_2 catalysts," *Journal of Photochemistry and Photobiology A*, vol. 108, no. 1, pp. 79–84, 1997.

[15] W. Li, Y. Wang, H. Lin et al., "Band gap tailoring of Nd^{3+}-doped TiO_2 nanoparticles," *Applied Physics Letters*, vol. 83, no. 20, pp. 4143–4145, 2003.

[16] Y. Gai, J. Li, S.-S. Li, J.-B. Xia, and S.-H. Wei, "Design of narrow-gap TiO_2: a passivated codoping approach for enhanced photoelectrochemical activity," *Physical Review Letters*, vol. 102, no. 3, Article ID 036402, 2009.

[17] H. Liu, Z. Lu, L. Yue et al., "(Mo+N) codoped TiO_2 for enhanced visible-light photoactivity," *Applied Surface Science*, vol. 257, no. 22, pp. 9355–9361, 2011.

[18] J. Yang, J. Dai, and J. Li, "Synthesis, characterization and degradation of Bisphenol A using Pr, N co-doped TiO_2 with highly visible light activity," *Applied Surface Science*, vol. 257, no. 21, pp. 8965–8973, 2011.

[19] H. Gao, B. Lu, F. Liu, Y. Liu, and X. Zhao, "Photocatalytical properties and theoretical analysis of N, Cd-codoped TiO_2 synthesized by thermal decomposition method," *International Journal of Photoenergy*, vol. 2012, Article ID 453018, 9 pages, 2012.

[20] T. Umebayashi, T. Yamaki, H. Itoh, and K. Asai, "Analysis of electronic structures of 3d transition metal-doped TiO_2 based on band calculations," *Journal of Physics and Chemistry of Solids*, vol. 63, no. 10, pp. 1909–1920, 2002.

[21] K.-S. Ahn, Y. Yan, S. Shet, T. Deutsch, J. Turner, and M. Al-Jassim, "Enhanced photoelectrochemical responses of ZnO films through Ga and N codoping," *Applied Physics Letters*, vol. 91, no. 23, Article ID 231909, 2007.

[22] W. Zhu, X. Qiu, V. Iancu et al., "Band gap narrowing of titanium oxide semiconductors by noncompensated anion-Cation codoping for enhanced visible-Light photoactivity," *Physical Review Letters*, vol. 103, no. 22, Article ID 226401, 2009.

[23] P. Romero-Gomez, A. Borras, A. Barranco, J. P. Espinos, and A. R. Gonzalez-Elipe, "Enhanced photoactivity in bilayer films with buried rutile-anatase heterojunctions," *ChemPhysChem*, vol. 12, no. 1, pp. 191–196, 2011.

[24] P. Deák, B. Aradi, and T. Frauenheim, "Band lineup and charge carrier separation in mixed rutile-anatase systems," *Journal of Physical Chemistry C*, vol. 115, no. 8, pp. 3443–3446, 2011.

[25] K. Y. Jung and S. B. Park, "Anatase-phase titania: preparation by embedding silica and photocatalytic activity for the decomposition of trichloroethylene," *Journal of Photochemistry and Photobiology A*, vol. 127, no. 1–3, pp. 117–122, 1999.

[26] J. Zhu, W. Zheng, B. He, J. Zhang, and M. Anpo, "Characterization of Fe-TiO_2 photocatalysts synthesized by hydrothermal method and their photocatalytic reactivity for photodegradation of XRG dye diluted in water," *Journal of Molecular Catalysis A*, vol. 216, no. 1, pp. 35–43, 2004.

[27] J. Yu, M. Zhou, H. Yu, Q. Zhang, and Y. Yu, "Enhanced photoinduced super-hydrophilicity of the sol-gel-derived TiO_2 thin films by Fe-doping," *Materials Chemistry and Physics*, vol. 95, no. 2-3, pp. 193–196, 2006.

[28] W. Q. Peng, M. Yanagida, and L. Y. Han, "Rutile-anatase TiO_2 photoanodes for dye-sensitized solar cells," *Journal of Nonlinear Optical Physics and Materials*, vol. 19, no. 4, pp. 673–679, 2010.

[29] G. Liu, X. Yan, Z. Chen et al., "Synthesis of rutile-anatase core-shell structured TiO_2 for photocatalysis," *Journal of Materials Chemistry*, vol. 19, no. 36, pp. 6590–6596, 2009.

[30] T. Miyagi, M. Kamei, T. Mitsuhashi, T. Ishigaki, and A. Yamazaki, "Charge separation at the rutile/anatase interface: a dominant factor of photocatalytic activity," *Chemical Physics Letters*, vol. 390, no. 4–6, pp. 399–402, 2004.

[31] W. Ren, Z. Ai, F. Jia, L. Zhang, X. Fan, and Z. Zou, "Low temperature preparation and visible light photocatalytic activity of mesoporous carbon-doped crystalline TiO_2," *Applied Catalysis B*, vol. 69, no. 3-4, pp. 138–144, 2007.

[32] H. Irie, Y. Watanabe, and K. Hashimoto, "Carbon-doped anatase TiO_2 powders as a visible-light sensitive photocatalyst," *Chemistry Letters*, vol. 32, no. 8, pp. 772–773, 2003.

[33] J. L. Gole, J. D. Stout, C. Burda, Y. Lou, and X. Chen, "Highly efficient formation of visible light tunable TiO_2-xNx photocatalysts and their transformation at the nanoscale," *Journal of Physical Chemistry B*, vol. 108, no. 4, pp. 1230–1240, 2004.

[34] C. S. Gopinath, "Comment on "photoelectron spectroscopic investigation of nitrogen-doped titania nanoparticles"," *Journal of Physical Chemistry B*, vol. 110, no. 13, pp. 7079–7080, 2006.

[35] C. Burda and J. Gole, "Reply to "comment on 'photoelectron spectroscopic investigation of nitrogen-doped titania nanoparticles'"," *Journal of Physical Chemistry B*, vol. 110, no. 13, pp. 7081–7082, 2006.

[36] J. F. Molder, W. F. Stickle, P. E. Sobol, and K. D. Bomben, *Handbook of X-Ray Photoelectron Spectroscopy*, Perkin-Elmer, Eden Prairie, Minn, USA, 2nd edition, 1992.

[37] C. D. Wagner, W. M. Riggs, L. E. Davis, J. F. Moulder, and G. E. Muilenberg, *Handbook of Xray Photoelectron Spectroscopy*, PerkinElmer Corp., Physical Electronics Division, Eden Prairie, Minn, USA, 1979.

[38] J. Li, J. Xu, W.-L. Dai, H. Li, and K. Fan, "Direct hydro-alcohol thermal synthesis of special core-shell structured Fe-doped titania microspheres with extended visible light response and enhanced photoactivity," *Applied Catalysis B*, vol. 85, no. 3-4, pp. 162–170, 2009.

[39] J. Wang, D. N. Tafen, J. P. Lewis et al., "Origin of photocatalytic activity of Nitrogen-doped TiO_2 nanobelts," *Journal of the American Chemical Society*, vol. 131, no. 34, pp. 12290–12297, 2009.

[40] J. Yu, Q. Xiang, and M. Zhou, "Preparation, characterization and visible-light-driven photocatalytic activity of Fe-doped titania nanorods and first-principles study for electronic structures," *Applied Catalysis B*, vol. 90, no. 3-4, pp. 595–602, 2009.

[41] W. Choi, A. Termin, and M. R. Hoffmann, "The role of metal ion dopants in quantum-sized TiO_2: correlation between photoreactivity and charge carrier recombination dynamics," *Journal of Physical Chemistry*, vol. 98, no. 51, pp. 13669–13679, 1994.

[42] K. Tan, H. Zhang, C. Xie, H. Zheng, Y. Gu, and W. F. Zhang, "Visible-light absorption and photocatalytic activity in molybdenum- and nitrogen-codoped TiO_2," *Catalysis Communications*, vol. 11, no. 5, pp. 331–335, 2010.

[43] T. Ihara, M. Miyoshi, Y. Iriyama, O. Matsumoto, and S. Sugihara, "Visible-light-active titanium oxide photocatalyst realized by an oxygen-deficient structure and by nitrogen doping," *Applied Catalysis B*, vol. 42, no. 4, pp. 403–409, 2003.

[44] I. Nakamura, N. Negishi, S. Kutsuna, T. Ihara, S. Sugihara, and K. Takeuchi, "Role of oxygen vacancy in the plasma-treated TiO_2 photocatalyst with visible light activity for NO removal," *Journal of Molecular Catalysis A*, vol. 161, no. 1-2, pp. 205–212, 2000.

[45] I. Justicia, P. Ordejón, G. Canto et al., "Designed self-doped titanium oxide thin films for efficient visible-light photocatalysis," *Advanced Materials*, vol. 14, no. 19, pp. 1399–1402, 2002.